Polymorphism of V-amylose cocrystallized with aliphatic diols

Cong Anh Khanh Le, Luc Choisnard, Denis Wouessidjewe, Jean-Luc Putaux

Published in **Polymer** *213* (2021), 123302 – https://doi.org/10.1016/j.polymer.2020.123302

Polymorphism of V-amylose cocrystallized with aliphatic diols

Cong Anh Khanh Le [a], Luc Choisnard [b], Denis Wouessidjewe [b], Jean-Luc Putaux [a,*]

[a] *Univ. Grenoble Alpes, CNRS, CERMAV, F-38000 Grenoble, France*

[b] *Univ. Grenoble Alpes, CNRS, DPM, F-38000 Grenoble, France*

* corresponding author:

Email: jean-luc.putaux@cermav.cnrs.fr

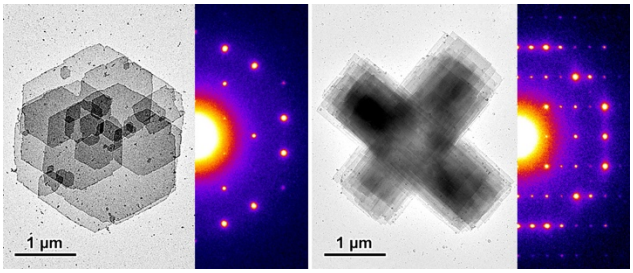

Table of Content Graphic - For Table of Contents use only

ABSTRACT

Chain-folded lamellar crystalline complexes of amylose with aliphatic diols were prepared and characterized by transmission electron microscopy as well as electron and X-ray diffraction. Four allomorphs were identified, depending on the complexing diol and crystallization conditions, that consisted of orthorhombic lattices of antiparallel 6- or 7-fold amylose single helices. Straight-chain *n*-diols (ethane-1,2-diol, butane-1,4-diol, hexane-1,6-diol) yielded 6-fold helical complexes regardless the length of the linear chain, whereas a bulkier branched diol (2-methylpentane-2,4-diol) induced the formation of 7-fold helices. Butane-1,3-diol, that contains a straight carbon chain with one end and one side hydroxyl group, induced both 6- and 7-fold helical conformations depending on the crystallization conditions. When a diol induced more than one allomorph, an adequate control of its concentration and crystallization temperature allowed targeting a specific crystalline form. Upon drying, all allomorphs were converted into more compact pseudo-hexagonal structures. The dried form of a given complex generally retained the same helical conformation as the hydrated one.

Keywords: V-amylose, diol, cocrystal, polymorphism

1. Introduction

Amylose, the mostly linear homopolymer of α(1–4)-linked D-glucosyl units extracted from native starch, cocrystallizes with a wide variety of small organic compounds [1,2]. These compounds are referred to as V-amylose and contain amylose single helices with guest molecules located inside the helices, in-between or both [3]. The V-amylose inclusion complexes present a number of interesting properties and potential applications, for instance in the food and pharmaceutical industries [4,5]. Complexing agents such as *n*-butanol, thymol or menthone have been used for the fractionation of native starch into its amylopectin and amylose constituents [6-8]. Amylose complexes have been shown to efficiently encapsulate flavoring compounds [9,10] or fatty acids in order to modulate the rheological, taste and hydrolysis properties of starch-based matrices [11-13]. Their potential as delivery systems of bioactive agents has also been evaluated [14-17].

Depending on the complexing agent and crystallization conditions, several V-amylose allomorphs have been reported in the literature that can be readily identified by their X-ray powder diffraction pattern. So far, it has not been possible to grow large crystals amenable to a three-dimensional molecular structure determination by single crystal X-ray diffraction methods. Nevertheless, V-amylose can be easily crystallized from dilute aqueous solution (0.05–0.1 wt%) in the form of *ca.* 10 nm-thick lamellar single crystals with a lateral size up to a few micrometers. In these, the amylose chains are organized in helices, with their axis perpendicular to the base plane of the lamellae. When the chain length of amylose exceeds the lamellar thickness, a regular chain folding mechanism occurs, similar to the one described for flexible synthetic polymers [18-20]. For the not-so-flexible amylose molecule, chain folding is readily favored by a band-flip mechanism that is specific of α(1–4) glucans [21]. The V-amylose crystals yield high-quality electron diffraction, providing rich diffraction datasets useful for structural analysis [22].

A generic classification of V-amylose allomorphs can be done according to the number of glucosyl units per helical turn (6, 7 or 8) but these main classes contain subfamilies with specific morphological and structural signatures [22]. The V6 family comprises three crystal types: the pseudo-hexagonal $V6_I$ (or V_h), typically formed with linear alcohols [23,24] and fatty acids [25,26], the orthorhombic $V6_{II}$ prepared with $V_{n\text{-butanol}}$ [27] and a pseudo-tetragonal V6 reported for complexes with dimethyl sulfoxide (DMSO) [28], ethylenediamine [29], and glycerol [30]. Although a $V6_{III}$ allomorph is mentioned in some works [31,32], the corresponding structure has been shown to be based on 7-fold helices [33]. Therefore, in the following, the V6 complexes isomorphous to V_{DMSO} and $V_{glycerol}$ will be referred to as $V6_{III}$. Seven-fold amylose helices have been found in two allomorphs: one, with an orthorhombic unit cell, has been prepared with propan-2-ol [33,34], some fatty acids [26], many alcohols and aroma compounds [9,35,36], and

the other, recently identified for complexes with bicyclic compounds, with a pseudo-hexagonal unit cell [37]. The latter will be referred to as $V7_I$ and the former as $V7_{II}$ [37]. Quinoline and naphthalen-1-ol (1-naphthol) induce the formation of V8 helices organized in a tetragonal unit cell [36,38,39] while another V8 form, which structure has not been clearly described yet, has been reported for complexes with 2-hydroxybenzoic (salicylic) acid [14,40].

V-amylose crystallosolvates also contain a number of water molecules and dehydration / desolvation can induce structural transitions. The drying of the $V6_I$ and the $V6_{II}$ crystals prepared with fatty acids or aliphatic alcohols results in the pseudo-hexagonal anhydrous $V6_a$ [27,35,41-43]. However, it was shown that even after a strong dehydration treatment (heating under vacuum and over phosphorus pentoxide), a number of water molecules were still present in the crystal [44]. Similarly, upon drying, $V7_I$ and $V7_{II}$ were converted to a compact pseudo-hexagonal $V7_a$ [35,37,40,43,45]. A $V8_a$ structure has been reported after drying of a V8 complex with salicylic acid [40]. The data suggested that it might also be pseudo-hexagonal. In all aforementioned cases, drying induced a compaction of the helices but the helicity was maintained.

A number of authors have proposed that the helix diameter depended on the cross-sectional diameter of the guest [19,31,33,35,43,45-47]. More specifically, V6 complexes have been obtained with molecules containing a main linear carbon chain, regardless of the functional groups, while V7 and V8 complexes have been prepared with bulkier compounds containing branched chains or ring structures. Besides, Takeo and Kuge [35] and Takeo et al. [43] mentioned that the length of the linear chain of fatty acids and ketones were also key factors controlling the helix diameter. However, our recent structural investigation of V-amylose complexes with a series of straight-chain saturated fatty acids (from C3 to C20) revealed that all the tested guests yielded V6 or V7 structures, depending on the crystallization conditions [26]. In addition, some complexing agents such as acetone, DMSO, fatty acids, propan-2-ol, quinoline or salicylic acid induce more than one amylose helical conformation by varying the crystallization conditions [14,29,32,43]. The actual role of the guest molecule dimension can thus be questioned and other factors that control the conformation and packing arrangement in V-amylose allomorphs should be investigated. To our knowledge, such question has not been addressed so far for complexes prepared with aliphatic diols. Kowblansky [49] studied the thermal properties of complexes prepared with decane-1,10-diol and decane-1,12-diol but did not characterize the corresponding structure, while Helbert [32] reported on the formation of $V6_I$ with linear ethane-1,2-diol, propane-1,3-diol and butane-1,4-diol.

This paper focuses on the formation of complexes of V-amylose with aliphatic diols differing by the carbon skeleton (linear or branched), chain length and position of the hydroxyl groups. The morphology and structure of model lamellar single crystals prepared from dilute amylose solutions

were characterized by transmission electron microscopy (TEM) as well as electron and X-ray diffraction (ED and XRD, respectively). The influence of the guest molecule topology, its concentration and the crystallization temperature on the complex formation and resulting crystal structures were investigated, as well as the structural transitions induced upon drying.

2. Experimental section

2.1. Amylose and diols

Potato amylose was purchased from Sigma-Aldrich and further purified in laboratory as previously reported [26]. According to the method described in Supplementary Data **Fig. S1,** the chain length distribution was determined by size exclusion chromatography (SEC) with multi-angle laser light scattering (MALLS) from a solution of amylose dissolved in LiCl/1,3-dimethyl-2-imidazolidinone (LiCl/DMAc). The number- and weight-average degrees of polymerization were found to be $\overline{DP_n}$ = 928 and $\overline{DP_w}$ = 2514, respectively, with a polydispersity index $P = \overline{DP_w}/\overline{DP_n} = 2.7$. Ethane-1,2-diol (EDIOL), butane-1,3-diol (BBIOL), butane-1,4-diol (BDIOL), hexane-1,6-diol (HDIOL), and 2-methylpentane-2,4-diol (MPDIOL) were purchased from Sigma-Aldrich (**Scheme 1**).

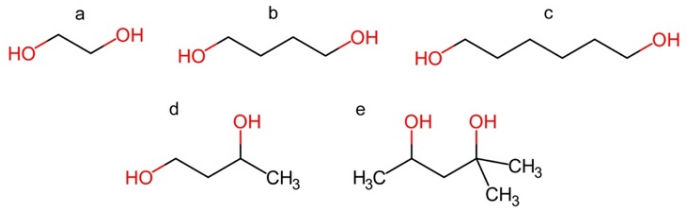

Scheme 1: Molecular structure of the diols tested in this study: a) ethane-1,2-diol (EDIOL); b) butane-1,4-diol (BDIOL); c) hexane-1,6-diol (HDIOL); d) butane-1,3-diol (BBIOL); e) 2-methylpentane-2,4-diol (MPDIOL) (drawn with MarvinSketch [50]). Three-dimensional molecular models are shown in Supplementary Data **Fig. S2**.

2.2. Crystallization protocols and drying procedure

Aqueous amylose dispersions (10 mg in 10 mL) were submitted to nitrogen bubbling during 20 min, autoclaved in an oil bath at 160 °C for 30 min to erase all memory of crystallization, and cooled down to 90 °C. The amount of added diol and the way it was mixed with amylose depended on some of its physical properties. All diols were liquid at room temperature, except HDIOL (melting temperature: 43 °C). All diols were miscible with water except HDIOL and MPDIOL that were partly soluble. A predetermined amount of preheated diol (10–80 vol% EDIOL, BBIOL and BDIOL; 0.5–20 wt% HDIOL and 1–20 vol% MPDIOL) was then added to the amylose solution at 90 °C. After a brief manual homogenization, the mixtures were kept at a given temperature (25-

75 °C) during one week and cooled down to room temperature or, after mixing, were allowed to slowly cool down in a Dewar vessel. When the incubation at 40–75 °C did not induce crystallization after one week, especially with a low diol concentration, the mixture was cooled down to 25 °C and monitored until a solid residue was formed. In all cases, the crystallized fractions were characterized shortly after collection. For drying experiments, the complexes were kept under primary pump vacuum at room temperature. Samples were taken after pumping periods of one day up to several weeks and analyzed by XRD. The sample was considered as "dry" when a stable XRD pattern was achieved. The term "partially dried " will refer to the intermediate state between the fully hydrated/solvated and dry states, during which changes in XRD profiles were still observed.

2.3. X-ray diffraction (XRD)

The crystal suspensions were centrifuged for 10 min at 13400 rpm (12000 *g*) and the pellets deposited on a 7-µm nylon bolting cloth (SaatiTech), laying on top of blotting paper. After absorption of the excess solvent, the crystals were either equilibrated for several days in a closed chamber equilibrated with a 95% relative humidity (RH) or dried in primary pump vacuum. Thin strips of the resulting films were inserted into 1 mm (outer diameter) glass capillaries which were immediately flame-sealed. The specimens were X-rayed in transmission in a Warhus vacuum camera with a Ni-filtered CuKα radiation (λ = 0.1542 nm), using a Philips PW3830 generator operating at 30 kV and 20 mA. Two-dimensional diagrams were recorded on Fujifilm image plates during 2 h and read with a Fujifilm BAS 1800-II bioimaging analyzer. XRD profiles were calculated by rotational averaging of the 2D patterns. The XRD data were calibrated using calcite and the unit cell parameters were refined using the Celref program [51].

2.4. Transmission electron microscopy (TEM) and electron diffraction (ED)

Droplets of dilute crystal suspensions were deposited on glow-discharged carbon-coated grids. After 2 min, the liquid in excess was wicked off with a filter paper and the preparation allowed to dry. The specimens were observed with a Thermo Scientific Philips CM200 'Cryo' microscope operating at 200 kV. For electron diffraction, after the last traces of liquid had visually disappeared from the carbon film surface, the TEM grids were mounted on a Gatan 626 specimen cryoholder and immediately fast-frozen into liquid nitrogen. Once in the microscope, the holder was cooled down with liquid nitrogen and the crystals were observed under low dose illumination at -177 °C. Images and selected area ED patterns were recorded with a TVIPS TemCam F216 camera. The ED diagrams were calibrated using a gold-coated carbon film as standard. In the following, "base-plane ED patterns" will refer to patterns recorded along the [001] *c*-axis of the crystal structure, i.e. perpendicular to the *(a,b)* plane of the lamellae and parallel to the axis of the amylose helices.

3. Results and discussion

3.1. Morphology and crystal structure

The lamellar crystals formed in the presence of linear or branched diols (**Scheme 1**) under different crystallization conditions were divided into four types. The first type of crystal, with a more or less hexagonal shape and favoring a dislocation-centered spiral growth, was obtained with EDIOL, BDIOL, HDIOL and BBIOL (**Fig. 1a-d**, Supplementary Data **Fig. S3**). The base-plane ED patterns recorded on frozen-hydrated crystals (**Fig. 1e**) and the XRD patterns recorded on hydrated crystal mats (**Fig. 1f**) were almost identical to those reported for $V6_I$ prepared in the presence of linear alcohols [23,32] and fatty acids [26,32]. They were indexed on the basis of a hexagonal unit cell with space group $P6_522$ [23] or a pseudo-hexagonal orthorhombic unit cell with space group $P2_12_12_1$ [24]. The two unit cells have in common the close packing of 6-fold left-handed amylose helices onto a hexagonal lattice, but they differ in the arrangement of the up and down chains, which would be statistically random in the hexagonal unit cell [23] and regularly alternating in the orthorhombic unit cell (**Fig. 6b**) [24]. Our present data does not allow to distinguish between the two space groups. Consequently, for simplicity, we will only refer to the pseudo-hexagonal orthorhombic unit cell in the following. The average unit cell parameters determined by XRD (a = 1.37 nm, $b = a\sqrt{3}$ = 2.37 nm, and c = 0.81 nm) are in good agreement with those determined from ED patterns (a = 1.34 nm, b = 2.32 nm) (**Table 1**) and those reported by other authors for the $V6_I$ allomorph [23,32]. The complexing agent would only be located inside the helix cavity, since the interhelical space is too small [25].

Table 1. Average unit cell parameters (nm) of different allomorphs of amylose cocrystallized with diols, determined from base-plane electron diffraction (ED) and powder X-ray diffraction (XRD) patterns. "-": not determined.

Allomorph	ED		XRD		
	a	*b*	*a*	*b*	*c*
$V6_I$ [a,g]	1.34 ± 0.02	2.32 ± 0.02	1.37 ± 0.00	2.37 ± 0.00	0.81 ± 0.01
$V6_{II}$ [a,h]	2.68 ± 0.03	2.72 ± 0.02	2.66 ± 0.00	2.72 ± 0.01	0.79 ± 0.01
$V6_{III}$ [b,h]	2.68 ± 0.02	2.68 ± 0.02	2.71 ± 0.00	2.71 ± 0.00	-
$V6_a$ [c,g]	1.30 ± 0.00	2.25 ± 0.00	1.31 ± 0.02	2.27 ± 0.03	0.81 ± 0.01
$V6_a$ [d,h]	2.25 ± 0.00	2.60 ± 0.00	2.29 ± 0.00	2.64 ± 0.00	0.81 ± 0.01
$V7_I$ [a,g]	1.50 ± 0.00	2.60 ± 0.00	1.50 ± 0.00	2.60 ± 0.00	0.79 ± 0.00
$V7_{II}$ [a,h]	2.79 ± 0.00	2.96 ± 0.00	2.83 ± 0.00	2.98 ± 0.01	-
$V7_a$ [e,g]	1.47 ± 0.00	2.55 ± 0.00	1.47 ± 0.00	2.55 ± 0.00	0.78 ± 0.00
$V7_a$ [f,h]	2.55 ± 0.00	2.94 ± 0.00	2.55 ± 0.00	2.94 ± 0.00	0.78 ± 0.00

[a] hydrated crystals.
[b] obtained by partial drying of $V6_{II}$ complexes.
[c] obtained by vacuum drying of $V6_I$ complexes.
[d] obtained by vacuum drying of $V6_{II}$ complexes.
[e] obtained by vacuum drying of $V7_I$ complexes.
[f] obtained by vacuum drying of $V7_{II}$ complexes.
[g] the unit cell contains 2 helices.
[h] the unit cell contains 4 helices.

The second type of crystal, obtained with BDIOL, HDIOL and BBIOL, occurred in the form of stacks of rectangular lamellae. Stacks were individual (**Fig. 2a** and **2d**) or existed as twins forming an angle of approximately 60 or 90° (**Fig. 2b** and **2c,** Supplementary Data **Fig. S4**). This morphology is similar to that previously described for the $V6_{II}$ allomorph obtained with fatty acids [26], *n*-butanol and *n*-pentanol [32,47]. The ED patterns recorded on hydrated stacks of lamellae perpendicularly to the *(a,b)* so-called base plane of the crystal, i.e. along the [001] *c*-axis, were unique, which means that all lamellae in a stack share a strict orientation relationship, characteristic of a homoepitaxial growth (**Fig. 2e**). Furthermore, ED and XRD patterns (**Fig. 2f**) recorded on hydrated specimens are typical of $V6_{II}$ complexes [32,48] and correspond to an orthorhombic unit cell with space group $P2_12_12_1$ (**Table 1**). The parameters measured from base-plane ED diagrams of complexes with different diols (a = 2.68 nm, b = 2.72 nm) were in good agreement with those calculated from XRD data (a = 2.65 nm, b = 2.72 nm and c = 0.79 nm). Helbert and Chanzy [27] proposed a model where the amylose chains are organized in antiparallel pairs of 6-fold amylose helices inside the orthorhombic unit cell (**Fig. 6c**). The guest and water molecules would be included in the helical cavity and between helices. Our a and b parameters are reversed with respect to those proposed by Helbert and Chanzy since, as proposed by Donnay [52], and to be consistent with all the other V-amylose allomorphs, we have used the convention that a would be smaller than b.

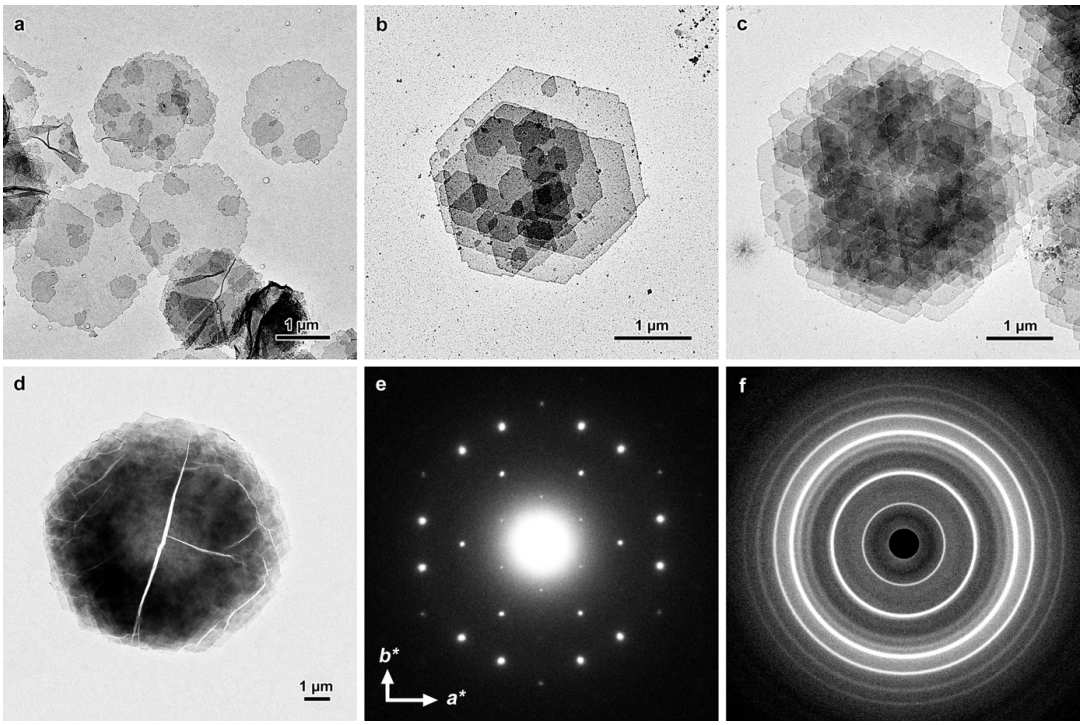

Fig. 1. The $V6_I$ allomorph: a-d) TEM images of V-amylose crystallized with BBIOL (a,b), EDIOL (c) and HDIOL (d); e) base-plane ED pattern recorded at low temperature from a frozen-hydrated V_{BBIOL} crystal; f) XRD powder diagram recorded from V_{HDIOL} crystals equilibrated at 95% RH.

The morphology of the third type of crystal was almost identical to that of $V6_I$ complexes regarding the hexagonal shape and dislocation-centered spiral growth (**Fig. 3a**). It was only observed with BBIOL. The ED (**Fig. 3b**) and XRD (**Figs. 3c**) patterns recorded on hydrated crystals were also qualitatively similar to those recorded from $V6_I$ crystals as they also exhibit a hexagonal symmetry. However, a careful calibration of the ED and XRD data showed that the reflections are globally located at smaller diffraction angles and were thus indexed on the basis of a larger pseudo-hexagonal orthorhombic unit cell ($a = 1.50$ nm, $b = a\sqrt{3} = 2.60$ nm and $c = 0.79$ nm) (**Table 1**). Assuming a lattice of close-packed amylose helices, a larger helix diameter of 1.50 nm can be deduced. This value is identical to that reported for the 7-fold helix in V-amylose complexes prepared with branched alcohols or fatty acids [19,43]. We have recently reported V-amylose crystals with a similar morphology and structure based on close-packed 7-fold helices in complexes prepared with bicyclic compounds such as borneol, camphor, *cis*-decahydro-1-naphthol or decahydro-2-naphthol [37]. We have proposed that this allomorph would be referred to as $V7_I$, by analogy with the close-packed $V6_I$, but also to differentiate it from another V7 allomorph, previously described by Nishiyama et al. [33], obtained with propan-2-ol, and referred to as $V7_{II}$ in the following. It is worth noting that, as previously suggested by Zaslow [45], a 7-fold helix cannot be crystallographically close-packed into a hexagonal unit cell. As a result, a pseudo-hexagonal unit cell with space group *P*1 has been used to describe the $V7_I$ structure (**Fig. 6f**). Due to the close packing, amylose helices are expected to be only separated by water molecules and the ligands would only be located inside the helix.

The fourth type of crystal, obtained with BBIOL and MPDIOL, occurred as rectangular lamellae frequently organized into flower-like aggregates (**Fig. 4a-b** and Supplementary Data **Fig. S5**). The ED patterns recorded on frozen-hydrated crystals (**Fig. 4c**) were indexed according to an orthorhombic unit cell with $a = 2.79$ nm and $b = 2.96$ nm, in agreement with the parameters calculated from XRD patterns ($a = 2.83$ nm and $b = 2.98$ nm. c could not be determined from the patterns) (**Fig. 4d**). Regarding their morphology and diffraction patterns, these crystals are isomorphous to the $V7_{II}$ crystals prepared with propan-2-ol [33,34], linear fatty acids [26], and many alcohols and aroma compounds [9,35,36]. The *c*-parameter of the unit cell was reported to be around 0.80 nm. The molecular model proposed by Nishiyama et al. [33] is presented in **Fig. 6g.** The orthorhombic unit cell contains four antiparallel left-handed 7-fold helices. The helices are not all close-packed which allows the guest molecules to be located both inside and between the helices.

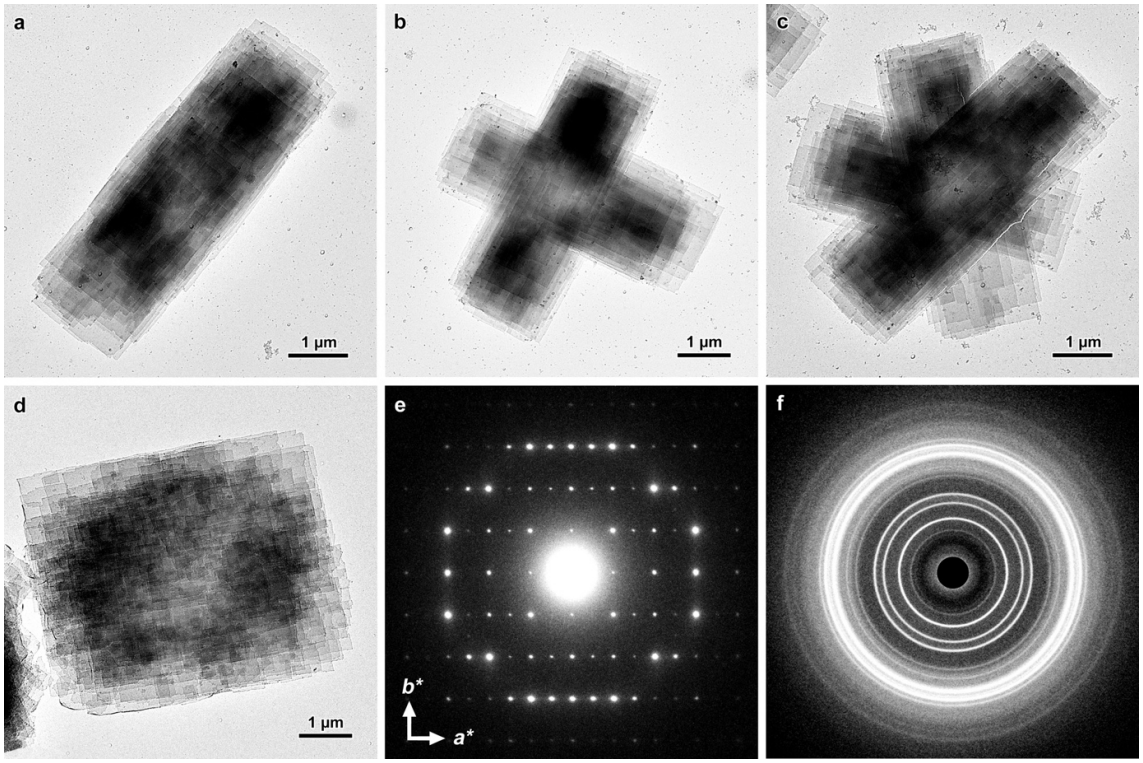

Fig. 2. The $V6_{II}$ allomorph: a-d) TEM images of V-amylose crystallized with BBIOL (a-c) and HDIOL (d); e) base-plane ED pattern recorded at low temperature from a frozen-hydrated V_{BBIOL} crystal; f) XRD powder diagram recorded from V_{BDIOL} crystals equilibrated at 95% RH.

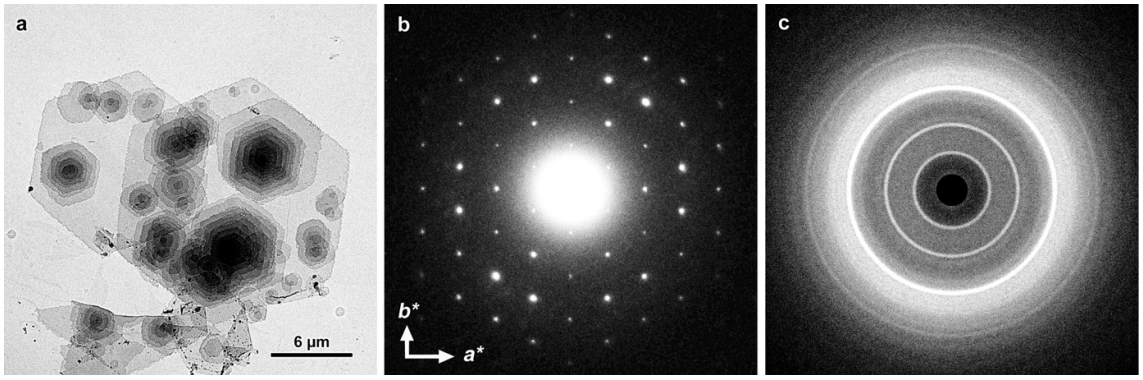

Fig. 3. The $V7_I$ allomorph: a) TEM image of V-amylose crystallized with BBIOL; b) base-plane pseudo-hexagonal ED pattern recorded at low temperature from a frozen-hydrated crystal; c) XRD powder diagram recorded from crystals equilibrated at 95% RH.

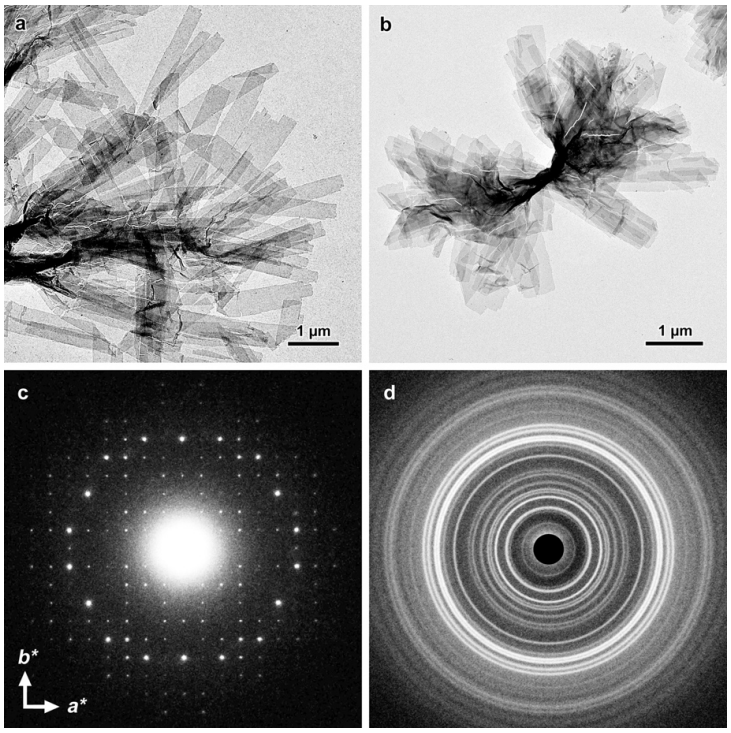

Fig. 4. The $V7_{II}$ allomorph: a,b) TEM image of V-amylose crystals prepared with MPDIOL (a) and BBIOL (b); c) base-plane ED pattern recorded at low temperature from a frozen-hydrated V_{BBIOL} crystal; d) XRD powder diagram recorded from V_{BBIOL} crystals equilibrated at 95% RH.

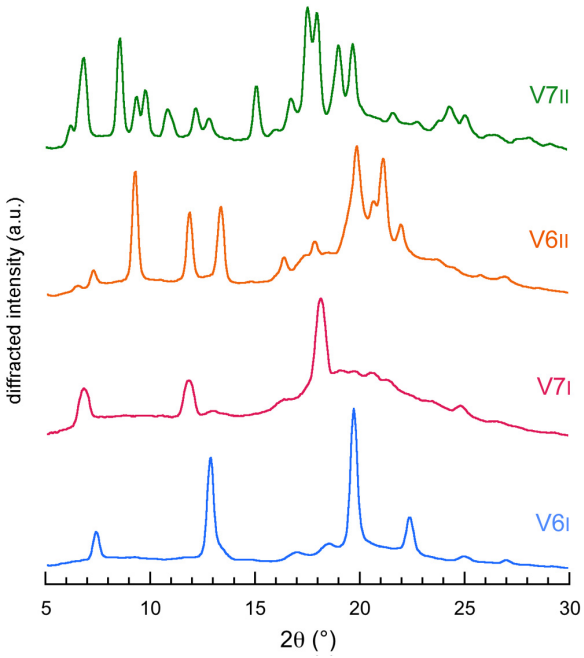

Fig. 5. Typical XRD profiles of V-type allomorphs that result from the direct crystallization of amylose in the presence of aliphatic diols. A given diol can induce the formation of different allomorphs (**Table 2** and Supplementary Data **Table S2**).

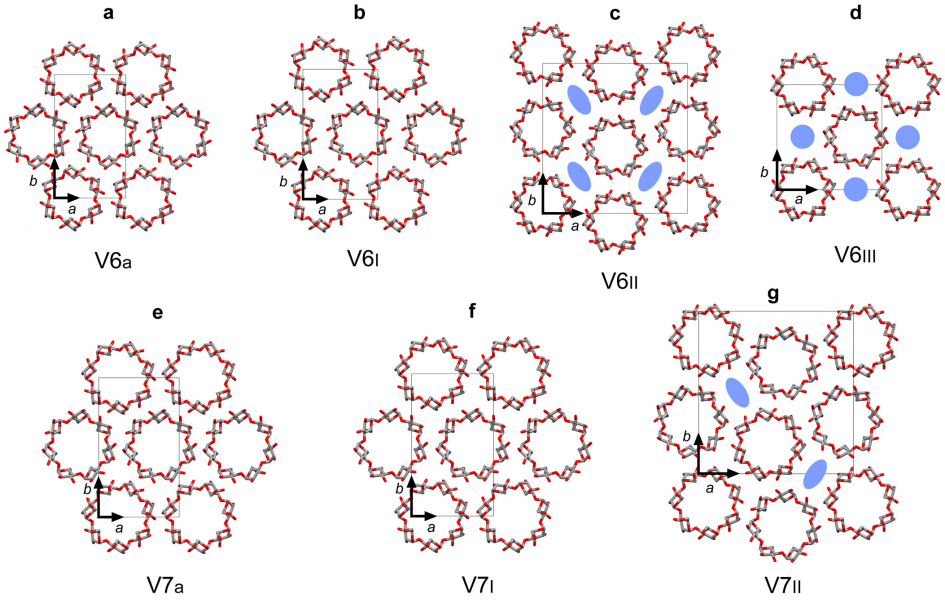

Fig. 6. Geometrical molecular models of the seven allomorphs of V-amylose considered in this study: a) $V6_a$, b) $V6_I$, c) $V6_{II}$, d) $V6_{III}$, e) $V7_a$, f) $V7_I$, g) $V7_{II}$. The helix packings are those proposed for V_a [42], V_h [24], $V_{butan\text{-}1\text{-}ol}$ [27], $V_{glycerol}$ [30], $V7_a$ [37], $V_{borneol}$ [37], and $V_{propan\text{-}2\text{-}ol}$ [33], respectively. In these base-plane projections along the helical *c*-axis, only the amylose helices have been drawn. Hydrogen atoms have been omitted for clarity. The conformation of the hydroxymethyl groups has been fixed as *gg* in all cases for simplicity and the helices were kept undistorted. The blue ovals mark the interhelical cavities. The unit cells have been superimposed on the models. Pseudo-hexagonal orthorhombic unit cells have been drawn in models a, b, e and f.

It must be noted that we did not observe the presence of the double-helical B-type allomorph in the XRD profiles. As seen in Supplementary Data **Fig. S6**, a typical signature of B-type is the strong peak located at $2\theta = 5.5°$, whose intensity depends on the specimen hydration [3]. Although the specimens were characterized just after cooling down to room temperature, the slow formation of B-type amylose from the uncomplexed amylose fraction after a long-term storage cannot be ruled out.

3.2. Crystal structure as a function of complexing diol

The series of diols was selected based on the carbon chain (straight or branched), chain length, and the position of hydroxyl groups on the chain (**Scheme 1**). The allomorphs characterized as a function of the selected diol, its concentration and the crystallization temperature are listed in **Table 2**. The corresponding XRD profiles are presented in Supplementary Data **Figs. S7-S9**. A general observation is that diols with a linear carbon chain and end hydroxyl groups induced the formation of V6 complexes, regardless of their chain length. More specifically, EDIOL induced the formation of $V6_I$ while BDIOL and HDIOL induced both $V6_I$ and $V6_{II}$. In contrast, the bulkier MPDIOL that contains a branched carbon backbone and side hydroxyl groups, only

yielded $V7_{II}$ complexes. Furthermore, with BBIOL, both 6- and 7-fold helical complexes were formed ($V6_I$, $V6_{II}$, $V7_I$ and $V7_{II}$). Indeed, BBIOL contains structural characteristics that are compatible with both 6-fold (a linear carbon chain, one end hydroxyl group) and 7-fold helical conformations (one side hydroxyl group).

The above results support the conclusions of previous studies that the conformation of V-amylose depends on the cross-sectional diameter of the guest molecule compared to the average diameter of the helical cavity of the amylose helix, *i.e.* around 0.45 and 0.55 nm for 6-and 7-fold helices, respectively [31,35,38,46,53]. These studies showed that complexing agents such as straight-chain *n*-alcohols and *n*-fatty acids, with a cross-sectional diameter similar to that of straight-chain *n*-diols (*ca.* 0.30 nm), favored 6-fold helices. V7 complexes were usually obtained with bulkier precipitants such as branched alcohols, aromatic hydrocarbons and monoterpenes with larger cross-sectional diameters (*ca.* 0.45–0.60 nm). Like BBIOL, some complexing agents such as propan-2-ol, acetone, methylethylketone or fatty acids induce both 6- and 7-fold helical conformations [26,32,35,43]. The linear carbon chain of these ligands contains a small side functional group (*e.g.* hydroxyl) or a larger end functional group (*e.g.* carboxyl). They exhibit intermediate cross-sectional diameters (0.36–0.45 nm) between those that are favorable for 6- and 7-fold helices. Since one turn of helix only consists of an integral number of glucosyl residues [35,53], a V6 or V7 allomorph, or both, can be formed depending on the crystallization conditions.

In addition to the different helical conformation, the different allomorphs contain a different helical packing. BDIOL, HDIOL and BBIOL induced 6-fold helices with two different packing arrangements: pseudo-hexagonal ($V6_I$) and orthorhombic ($V6_{II}$). A similar observation has also been reported for complexes with *n*-alcohols [32] as well as mono- and dicarboxylic acids [35,37]. Packing polymorphism seems to be much less prevalent for V7 complexes. So far, only BBIOL, *cis*-decahydro-1-naphthol and decahydro-2-naphthol have been shown to induce both $V7_I$ and $V7_{II}$ [37], while a large variety of ligands yield only $V7_{II}$ [9,35,36]. However, it is difficult to draw a conclusion regarding the formation of $V7_I$ as it is possible that the right set of crystallization conditions has not been yet found for each complexing agent.

3.3. Effect of crystallization conditions

As shown in **Table 2**, each diol exhibits a minimum concentration at which crystalline inclusion complexes with amylose are formed. The critical concentration is lower for diols with a longer chain or a lower water solubility. For example, only 1 wt% of HDIOL or 2.5 vol% MPDIOL is necessary to form complexes with amylose at 25 °C, compared to 40 vol% for

EDIOL. Besides, a higher concentration of diol allows the crystallization to be carried out at higher temperatures. Similar observations have been reported for fatty acids [26,32].

When a given diol such as BDIOL, HDIOL or BBIOL induced more than one crystal structure, the occurrence domain of each allomorph, defined by a set of conditions at which a specific allomorph crystallizes, can be independent or overlap onto one another (**Table 2**) [54]. Similar phenomena have been reported for V-amylose prepared with some fatty acids [26]. When the occurrence domain is unique, only one crystal type is obtained, that is the most thermodynamically stable. In contrast, when two domains overlap, two or more allomorphs are energetically close and thus crystallize under the same conditions. In that case, the occurrence of both allomorphs is controlled by a competition between thermodynamic stability and kinetic factors [54].

As shown in **Table 2** and illustrated by XRD profiles of V_{BDIOL}, V_{HDIOL} and V_{BBIOL} complexes in Supplementary Data **Fig. S8a-c**, the minimum diol concentration at which a given allomorph is formed can be arranged in the order: $V7_I > V6_I > V7_{II} > V6_{II}$. Similar observations have been reported for complexes with propan-2-ol, acetone and some fatty acids: $V6_I$ is preferred to $V7_{II}$ or $V6_{II}$ at a higher ligand concentration [26,32,43]. Indeed, $V6_{II}$ and $V7_{II}$ are less compact structures than $V6_I$ and $V7_I$. There is more interstitial space in $V6_{II}$ and $V7_{II}$ where water and ligands can be located to stabilize the structure. Indeed, as detailed in the following section, the drying of $V6_{II}$ and $V7_{II}$ complexes induced a transition to compact hexagonal structures. A high concentration of complexing agent possibly results in a dehydration of amylose and thus favors the formation of the more compact structures ($V6_I$ and $V7_I$). Moreover, the crystallization of V_{BBIOL} showed that 6-fold helices were preferred over 7-fold ones at lower ligand concentration in both orthorhombic ($V6_{II} < V7_{II}$) and compact pseudo-hexagonal structures ($V6_I < V7_I$). Hydration would thus play a significant role in governing the helical conformation of amylose.
Along with the control of diol concentration, variations in the crystallization temperature were explored. $V6_{II}$ and $V7_{II}$ complexes were obtained at relatively lower temperatures (25-40 °C) while $V6_I$ and $V7_I$ were formed within a wider range (25–75 °C) (**Table 2**). This observation agrees with our earlier findings on complexes with bicyclic organic compounds [40] or fatty acids [26]. We do not have any straightforward explanation to account for such a temperature influence toward the compactness of the crystals. It may be that a temperature increase favors a higher mobility of the amylose chains, which are therefore free to crystallize in compact packing of helices in close-contact arrangement. Supplementary Data **Fig. S9** shows XRD profiles of V_{BDIOL}, V_{HDIOL} and V_{BBIOL} complexes prepared with the same concentration of diol but at different temperatures. Some conclusions can be drawn: i) $V6_I$ was favored over $V6_{II}$ at higher temperatures (**Fig. S9a,b**); ii) $V7_{II}$ was favored over $V6_I$ and $V6_{II}$ at higher temperatures

Table 2. V-amylose allomorphs as a function of complexing diol, diol concentration (*C*) and incubation temperature. *C* is expressed in vol% for EDIOL, BDIOL, BBIOL and MPDIOL, and wt% for HDIOL. The amylose and diol solutions were mixed at 90 °C, then kept at a given temperature during one week and cooled down to room temperature, or allowed to slowly cool down in a Dewar vessel after mixing. For mixtures, the major and minor allomorphs are indicated. "-": no precipitation was observed and the solution remained clear; "n. t.": not tested.

	Incubation temperature (°C)				
C (%)	Slow cooling	25	40	60	75
Ethane-1,2-diol (EDIOL)					
30	n. t.	-	-	-	-
40	n. t.	$V6_I$	-	-	-
50	n. t.	$V6_I$	$V6_I$	-	-
60	n. t.	$V6_I$	$V6_I$	-	-
80	n. t.	$V6_I$	$V6_I$	$V6_I$	$V6_I$
Butane-1,4-diol (BDIOL)					
10	$V6_{II}$	-	-	-	-
15	$V6_{II}$	-	-	-	-
20	$V6_{II}$	$V6_{II}$	-	-	-
25	$V6_{II}$	$V6_{II}$	$V6_{II}$	-	-
30	$V6_I > V6_{II}$	$V6_{II} > V6_I$	$V6_I > V6_{II}$	-	-
35	$V6_I$	$V6_I$	V6I	-	-
40	$V6_I$	$V6_I$	$V6_I$	$V6_I$	-
50-60	$V6_I$	$V6_I$	$V6_I$	$V6_I$	$V6_I$
Hexane-1,6-diol (HDIOL)					
0.5	-	-	-	-	-
1.0	$V6_{II}$	$V6_{II}$	$V6_{II}$	-	-
2.5	$V6_{II}$	n. t.	$V6_{II}$	-	-
5.0	$V6_{II}$	n. t.	$V6_{II}$	$V6_{II}$	-
10.0	$V6_{II}$	n. t.	$V6_{II}$	$V6_{II} > V6_I$	-
15.0	$V6_{II}$	n. t.	$V6_{II}$	$V6_I > V6_{II}$	$V6_I$
20.0	$V6_I > V6_{II}$	n. t.	$V6_{II}$	$V6_I > V6_{II}$	$V6_I$
Butane-1,3-diol (BBIOL)					
20	-	-	-	-	-
25	$V6_{II} > V7_{II}$	-	-	-	-
30	$V7_{II} > V6_{II}$	$V6_{II} > V7_{II}$	$V7_{II}$	-	-
35	$V6_I > V7_{II}$, $V6_{II}$	$V6_{II} > V7_{II}$, $V6_I$	$V7_{II}$	-	-
40	$V6_I > V7_{II}$	$V6_I$	$V7_{II} > V6_I$	-	-
45	$V6_I > V7_{II}$	$V6_I$	$V6_I > V7_{II}$	-	-
50	$V6_I > V7_I$	$V6_I$	$V6_I$	$V6_I$, $V7_I$	-
60	$V7_I > V6_I$	$V6_I$, $V7_I$	$V6_I$, $V7_I$	$V7_I$	$V7_I$
2-Methylpentane-2,4-diol (MPDIOL)					
1.0	n. t.	-	-	-	-
2.5	n. t.	$V7_{II}$	-	-	-
5.0	n. t.	$V7_{II}$	$V7_{II}$	-	-
10.0	n. t.	$V7_{II}$	$V7_{II}$	$V7_{II}$	-
15.0	n. t.	$V7_{II}$	$V7_{II}$	$V7_{II}$	-
20.0	n. t.	$V7_{II}$	$V7_{II}$	$V7_{II}$	$V7_{II}$

(**Fig. S9c,d**); iii) $V7_I$ was favored over $V6_I$ at higher temperatures (**Fig. S9e,f**). Our previous work on complexes with fatty acids showed that $V6_I$ was preferred to both $V6_{II}$ and $V7_{II}$ at higher crystallization temperatures. The difference between the conclusions in the two studies may be due to the different chemical nature of the complexing agents or the difference in the range of tested temperatures. The crystallization of $V_{fatty\ acid}$ complexes was studied at $T \geq 40$ °C compared to $T \geq 25$ °C for V_{diol} complexes. Our results with diols also show that V-amylose complexes could be formed at 25 °C, especially with a relatively low concentration of ligand (**Table 2**). In this case, the prior incubation of the amylose / ligand mixture for one week at a higher temperature (40–75 °C), during which the crystallization did not occur, resulted in a higher yield of crystals, while a significant amorphous fraction was observed with shorter incubation times (not shown). A crystallization was thus successfully achieved when the amylose and ligands interacted for a sufficient time at higher temperature before cooling down. A similar phenomenon has been reported for complexes with fatty acids [26] and 1-naphthol [38].

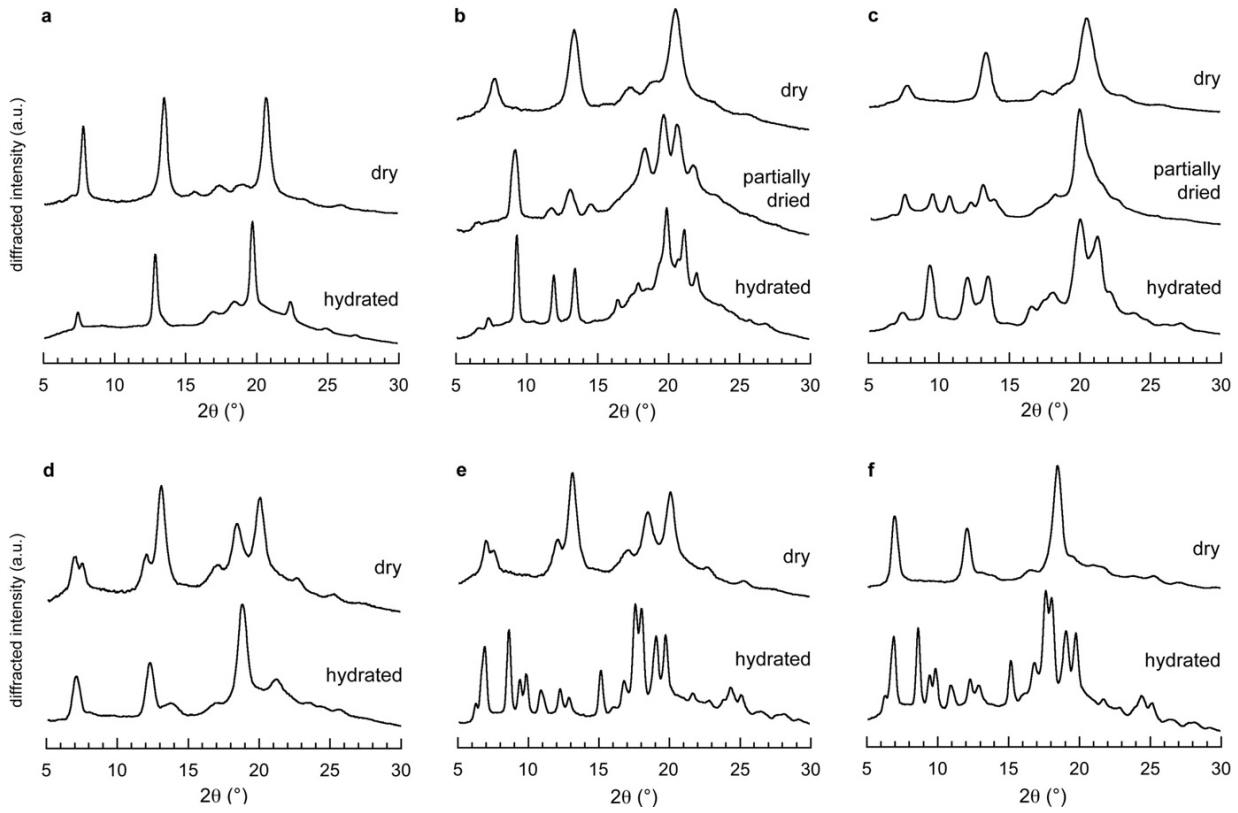

Fig. 7. Effect of drying on the XRD profiles of different V-amylose allomorphs prepared with BBIOL (a,b,d,e), HDIOL (c) and MPDIOL (f) in never-dried hydrated, partially dried and dry states. Upon drying, $V6_I$ was converted into $V6_a$ (a); $V6_{II}$ was first converted to $V6_{III}$, then $V6_a$ (b), or into a mixture of $V6_{II}$ and a second V6 form, then $V6_a$ (c); $V7_I$ was converted into a mixture of $V7_a$ and $V6_a$ (d); $V7_{II}$ was converted into a mixture of $V7_a$ and $V6_a$ (e), or only into $V7_a$ (f).

3.4. Effect of drying

Fig. 7 shows XRD profiles of the four V-amylose allomorphs obtained with BBIOL and MPDIOL and collected in the never-dried hydrated state and after drying. The profile of the extensively dried $V6_I$ complex is typical of the anhydrous $V6_a$ (**Fig. 7a**), in agreement with the results reported for $V6_I$ complexes obtained with linear alcohols and fatty acids [53,55]. This diagram can be indexed according to a pseudo-hexagonal orthorhombic unit cell with a = 1.32 nm, $b = a\sqrt{3}$ = 2.28 nm and c = 0.81 nm (**Table 1**). The slight difference in the unit cell parameters between $V6_I$ and $V6_a$ likely results from the release of water molecules from $V6_I$, which would reduce the interhelical space without altering the helical conformation and compact packing [48].

Like the $V6_I$ allomorph, $V6_{II}$ was also converted into the compact $V6_a$ after extended vacuum drying (**Figs. 7b,c**). Similar results have been reported for $V6_{II}$ prepared with butan-1-ol [48,56] and some dicarboxylic acids [43]. However, the structural transition occurred more slowly for the complexes with diols, allowing us to study intermediate structures. Different ED patterns were recorded from quench-frozen specimens of V_{BBIOL} crystals prepared from the same batch, which suggested that some preparations had partially dried before freezing and transfer into the microscope. **Fig. 8e** corresponds to the regular base-plane ED pattern of $V6_{II}$ crystals (**Fig. 8a**).

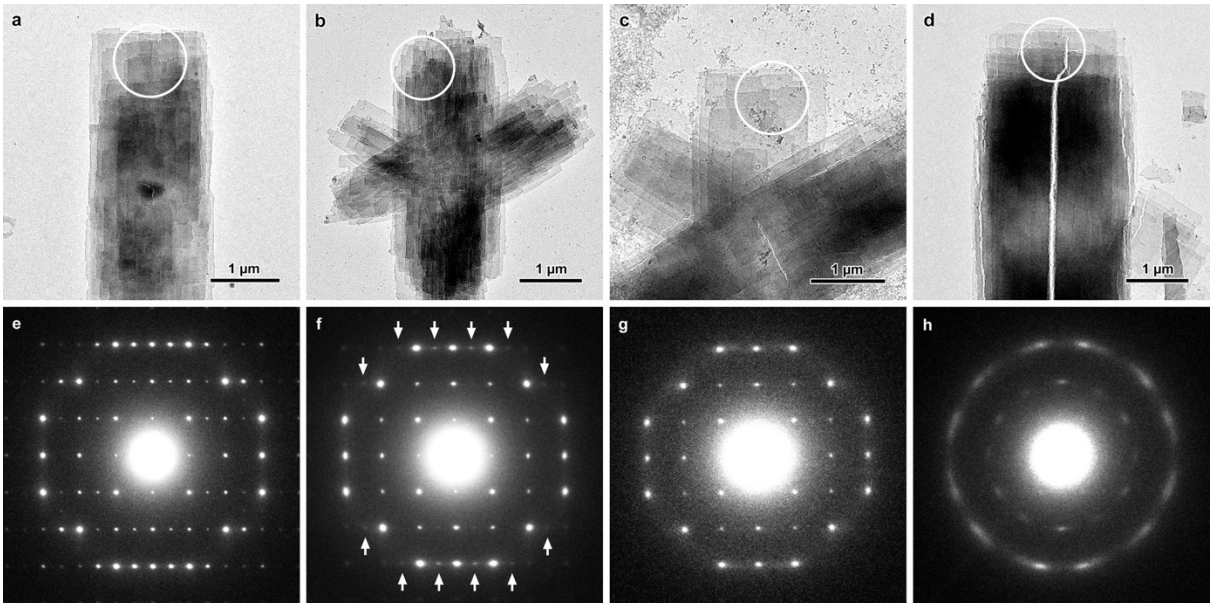

Fig. 8. Effect of partial and extensive drying on V_{BBIOL} crystals: TEM images (a-d) and corresponding properly oriented base-plane ED patterns (e-h) recorded at low temperature from frozen-hydrated crystals (e,f) and at room temperature (g,h), from the selected areas indicated by white circles. In f, the arrows indicate diffraction spots that still belong to the diagram in e. The $V6_{II}$ structure (e) is first converted to $V6_{III}$ after partial drying (g), then to $V6_a$ after extensive drying (h). The crystal in image d shows typical longitudinal drying cracks, as previously described by Helbert and Chanzy [27].

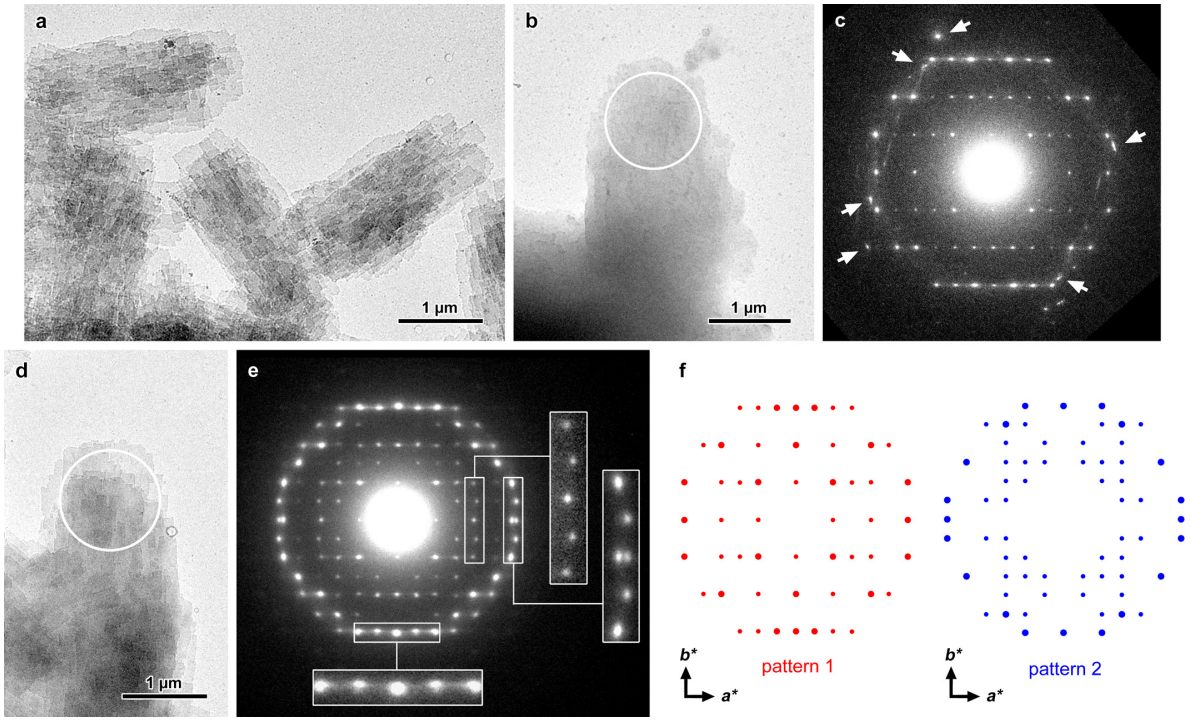

Fig. 9. a,b,d) TEM images of partially dried V_{HDIOL} crystals (a). In image b, a thin layer of mother liquor was frozen with the crystal, yielding extra spots (arrows) in the corresponding $V6_{II}$ ED pattern (c). The lamellae are more clearly visible in the crystal in image d. In the corresponding ED pattern (e), some reflections are not in perfect alignment and others appear to be split (enlarged insets). The diagram is the superimposition of two patterns: pattern 1 (in red) is that of $V6_{II}$ while pattern 2 (in blue) is similar to that of $V7_{II}$ (f). However, the cell parameters calculated for pattern 2 are significantly smaller than those of $V7_{II}$. ED patterns c and e have been recorded from the selected areas indicated by white circles in images b and d.

Some of the diffraction spots are still present in the pattern of **Fig. 8f** but the diagram in **Fig. 8g** is very similar to the one reported by Hulleman et al. [30] for $V6_{III}$ complexes with glycerol. The same observation was made for V_{BDIOL} complexes (Supplementary Data **Fig. S10**). The comparison of the XRD profiles recorded from a hydrated mat of V_{BBIOL} crystals and after a 1-h vacuum drying confirmed that the partial drying induced the formation of a structure that diffracted like $V6_{III}$ (**Fig. 7b**). This structure was rather stable and slowly converted into $V6_a$ over several weeks of drying (**Figs. 7b** and **8h**).

Fig. 7c shows the XRD profile of the V_{HDIOL} complex after a brief vacuum drying. The profile is not that of $V6_{III}$ as observed for V_{BBIOL} and V_{BDIOL} and contains peaks of the original $V6_{II}$ in addition to those of a different form. The base-plane ED patterns of quench-frozen V_{HDIOL} crystals are shown in **Fig. 9**. Two types of diagrams were recorded from crystals located on different regions on the TEM grid. For some crystals (**Fig. 9b**), the constituting lamellae were not clearly visible, suggesting that a thin film of mother liquor was frozen with the crystals that would thus be considered as fully hydrated / solvated. The corresponding ED pattern was that of $V6_{II}$ as

observed for V_{BBIOL} and V_{BDIOL} complexes (**Fig. 9c**). For other crystals where the lamellae were clearly visible (**Fig. 9d**), the diagram was more complex. A careful observation of the base-plane reflections showed that most rows contained misaligned spots (**Fig. 9e**). By isolating each set of spots, two different patterns were identified: pattern 1 was that of the original crystals, *i.e.* $V6_{II}$, while pattern 2 was similar to that of the $V7_{II}$ allomorph (**Figs. 9f** and **4c**). The a^* and b^* reciprocal axes in patterns 1 and 2 were perfectly aligned. However, using the unit cell parameters of $V6_{II}$ as a reference, those of pattern 2 were found to be a = 2.55 nm and b = 2.65 nm, values that are significantly lower than those of $V7_{II}$ (a = 2.79 nm and b = 2.96 nm). The occurrence of 7-fold helices in this structure is thus unlikely and since the starting allomorph was $V6_{II}$, we assumed that 6-fold helices were involved instead. The ED patterns recorded from the crystals after warming the specimen to room temperature were all similar to those with the superimposed patterns, although less resolved (not shown). A tentative model of the intermediate structure based on the arrangement of helices in the $V7_{II}$ allomorph but with 6-fold helices packed in a smaller unit cell is shown in **Fig. 10b**. Since no significant morphological change was observed in the crystals, we cannot determine whether some of the $V6_{II}$ constituting lamellae have been converted to the intermediate structure upon partial drying, or each lamella is a mosaic structure of locally converted domains. It must be noted that this structure has never been observed by direct crystallization of amylose and may be a new transitory organization of helices that occurs only under these drying conditions. The XRD profile of $V6_a$ was obtained after extended drying of the crystals (**Fig. 7c**).

The schemes in **Fig. 10** summarize the changes in the packing of amylose helices in the (*a,b*) plane resulting from the drying of $V6_{II}$ (**Fig. 10a** and **10b**) and $V7_{II}$ (**Fig. 10c**) complexes, taking into account the up and down orientation of the antiparallel helices. The helix arrangements proposed for $V6_a$ and $V6_{III}$ in the literature are given in **Fig. 10d**. Two constraints were considered to describe the partially dried and dry structures of chain-folded crystals: the local movements of helices were minimal and the up and down orientations were preserved during the transitions.

In the initial $V6_{II}$, amylose helices are organized in rows parallel to the *b*-axis of the unit cell and to the longer-dimension of the rectangular crystal, whereas the helices are staggered along the *a*-axis [27]. **Fig. 10a** illustrates a first drying pathway. Upon partial drying, amylose helices became aligned along both *a* and *b* axes resulting in a small increase of the *a*-parameter from 2.66 nm to 2.71 nm, while *b* remained unchanged. This transition is puzzling, although it is supported by the diffraction data from V_{BBIOL} (**Figs. 7b** and **8)** and V_{BDIOL} (Supplementary Data **Fig. S8**). The unit cell appears to be slightly larger than that of $V6_{II}$ while a compaction of the helices would be expected. This may suggest that during a first stage of drying the ligands reorganize in the interhelical space. Further experiments are necessary to fully understand this behavior by

analyzing the crystal structures of $V6_{II}$ complexes after equilibration at different relative humidities, or by monitoring the transition *in situ* on a shorter timescale. After extended drying, the amylose helices reorganized into a close-packed pseudo-hexagonal arrangement, with a slight decrease of the *b*-parameter (2.64 nm) but a significant decrease of *a* (2.29 nm), consistent with the formation of longitudinal cracks in the dried crystals (**Fig. 8d**) and in agreement with the observation of Helbert and Chanzy for $V_{butan\text{-}1\text{-}ol}$ complexes [27]. It must be noted that, although the helix arrangements in the (*a,b*) plane closely resemble those in $V6_{III}$ and $V6_a$, the distribution of up and down helices differ from those proposed for these allomorphs in the literature (**Fig. 10d**) [28,30]. Consequently, larger orthorhombic unit cells containing four amylose helices instead of two had to be considered.

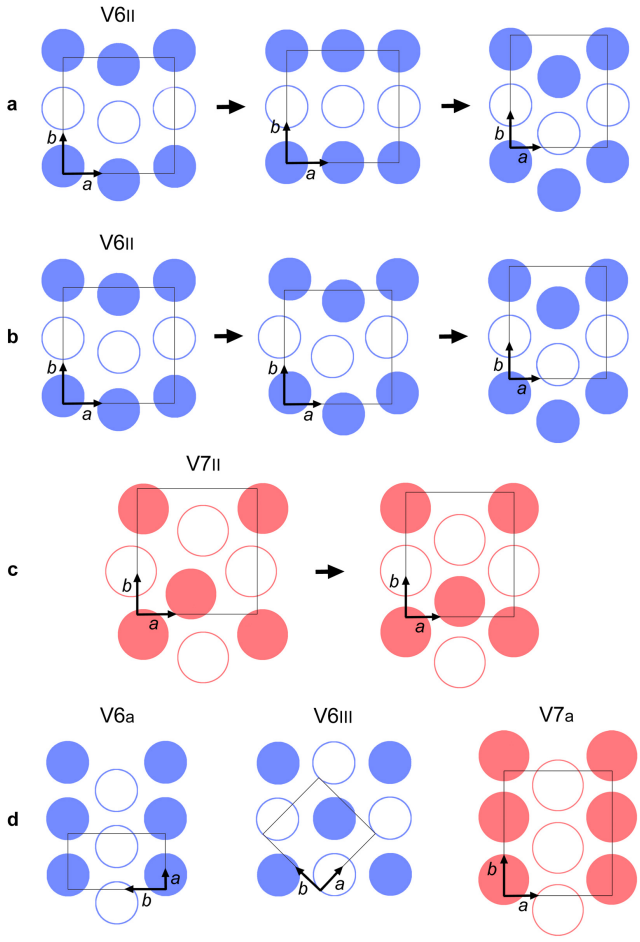

Fig. 10. Schemes describing tentative helix displacement upon drying of $V6_{II}$ and $V7_{II}$ complexes with diols, drawn in projection in the (*a,b*) plane: a) Drying of $V6_{II}$ from V_{BBIOL} and V_{BDIOL}; b) drying of $V6_{II}$ from V_{HDIOL}; c) drying of $V7_{II}$ from V_{MPDIOL}; d) structural models from the literature data: $V6_a$ [42], $V6_{III}$ [30] and $V7_a$ (deduced from $V7_I$ [37]). The starting models are based on those displayed in Figure 6. Up and down antiparallel amylose helices are schematized as disks and circles, respectively, whereas 6- and 7-fold helices are draw in blue and red, respectively.

A second drying pathway of $V6_{II}$ crystals is proposed in **Fig. 10b**, supported by the diffraction data of V_{HDIOL} crystals (**Figs. 7c** and **9**). The 6-fold helices would first reorganize into a pattern that resembles that of $V7_{II}$ but into a smaller unit cell, before settling into a close-packed pseudo-hexagonal arrangement. Again, although the positions of the helices of the intermediate structure are identical to those proposed for $V7_{II}$ in the (*a,b*) plane [33], the distribution of up and down orientations is different. After extended drying, the helices would adopt a pseudo-hexagonal close packing resembling that of $V6_a$.

Our analysis of the diffraction data from all intermediate and dry structures mainly relied on *hk*0 reflections, allowing to propose plausible distributions of helices in the (*a,b*) base plane. As seen in Supplementary Data **Tables S3** and **S4** in the case of V_{BBIOL} complexes, the number of XRD reflections indexed as *hkl* with $l \neq 0$ is very small. Therefore, due to this lack of information along the *c*-axis, the proposed models cannot be fully validated and the proposed orientation of helices relied on chain-folding constraints rather than symmetry considerations.

According to Helbert and Chanzy [27] the transition from $V6_{II}$ to $V6_a$ observed for complexes with butan-1-ol and pentan-1-ol would be due to the release of volatile ligands located in the interhelical space. However, such release is less likely for non-volatile complexing agents such as solid dicarboxylic acids [43]. This suggests that the departure of water rather than the complexing agent would also be a significant cause for the structural transition induced by drying. However, in our study, we did not have any quantitative evidence of the release of diol or water molecules from the crystals upon drying, although we can assume that the hygroscopic properties of diols, which should limit the departure of water, could be the reason for the slow transition observed for these complexes. The quantification of released molecules is thus an important aspect that must be addressed in a further study.

In the case of V7 crystals, different transition behaviors were noted for V_{BBIOL} and V_{MPDIOL}. On the one hand, extensively dried V_{MPDIOL} crystals ($V7_{II}$) yielded an XRD profile identical to that of $V7_a$ obtained by dehydration of complexes with propan-2-ol, branched alcohols, ketones, fatty acids and ring compounds (**Figs. 6e** and **7f**) [9,19,37,43,45,53]. The parameters of the pseudo-hexagonal orthorhombic unit cell are $a = 1.47$ nm, $b = a\sqrt{3} = 2.55$ nm and $c = 0.78$ nm (**Table 1**). Like in the dry close-packed structure based on 6-fold helices, the orientation of 7-fold helices is different from that expected from the drying of $V7_I$ crystals into $V7_a$ (**Fig. 10c** and **d**). On the other hand, characteristic reflections of both $V6_a$ and $V7_a$ were found in the XRD profile of the dried $V7_I$ and $V7_{II}$ complexes with BBIOL (**Fig. 7d** and **7e**, respectively), suggesting a partial helical transition from 7- to 6-fold. In previous studies, the transition from $V7_{II}$ to $V6_a$ only happened when the complexes were washed with aliphatic alcohols, followed by drying

[31,53,55]. Such treatments were shown to remove both water and guest molecules from the crystal. However, the transition from a 7- to a 6-fold helix in the V_{BBIOL} crystal agrees with the fact that BBIOL is compatible with both 6- and 7-fold helices. Indeed, such partial conversion was not observed for V_{MPDIOL} or many V7 complexes prepared with complexing agents that could not induce 6-fold helices [9,19,37,43,46,53]. Therefore, the effect of extensive drying on V7 complexes prepared with complexing agents such as acetone, propan-2-ol or butanone, that are also compatible with both 6- and 7-fold helices should be studied.

4. Conclusions

Amylose was successfully cocrystallized with aliphatic diols in the form of chain-folded lamellar crystals. Four allomorphs ($V6_I$, $V6_{II}$, $V7_I$ and $V7_{II}$) were identified from TEM images and diffraction data. On the one hand, the helical conformation of amylose was shown to depend on the cross-sectional diameter of the complexing agent. Linear *n*-diols yielded V6 complexes while bulkier diols with branched chain and/or side hydroxyl groups produced V7 crystals. BBIOL, with both a linear carbon chain and a side hydroxyl group induced both V6 and V7. On the other hand, BDIOL, HDIOL and BBIOL could form more than one allomorph, depending on the diol concentration and crystallization temperature. The minimum diol concentration at which a given allomorph was formed could be arranged in the order: $V7_I > V6_I > V7_{II} > V6_{II}$. For all complexes with the exception of V_{MPDIOL}, allomorphs with compact pseudo-hexagonal unit cells were favored at higher temperature and higher diol concentration.

Structural transitions occurred upon drying with a pathway that depended on the complexed diol. Transitions to more compact pseudo-hexagonal structures were also observed for all allomorphs after extensive drying. For most complexing agents, the helical conformation of amylose remained unchanged: $V6_I$ and $V6_{II}$ became $V6_a$, and $V7_{II}$ became $V7_a$. As an exception, both $V7_I$ and $V7_{II}$ formed with BBIOL were converted into a mixture of $V6_a$ and $V7_a$. The change in helical conformation may be related to the fact that, depending on the crystallization conditions, BBIOL induced 6- or 7-fold helices. The departure of water would play a significant role in the structural transitions, although the concomitant loss of ligand upon drying was not quantified. Therefore, rehydration / resolvation experiments should be conducted to see whether the transitions are reversible.

To complement this mainly descriptive study, further work will focus on several aspects. First, the ED and XRD data will be quantitatively analyzed to describe the molecular structures more precisely using crystallographic refinement methods. Second, the stoichiometry of the complexes in relation with the distribution of ligands and water molecules inside the helical

amylose scaffold will be determined. More detailed molecular models will help to understand how the crystal structure is stabilized and how different amylose conformations and helix arrangements are induced by a given ligand. Molecular dynamics calculations should also shed some light on the mechanisms at work during structural transitions, in particular upon drying the V-amylose complexes.

Acknowledgements

We thank LabEx Arcane (Investissements d'Avenir, grant agreement #ANR-11-LABX-0003-01) for funding the PhD thesis of C.A.K.L., the NanoBio-ICMG platform (FR 2607, Grenoble) for granting access to the Electron Microscopy facility, the Glyco@Alps program (Investissements d'Avenir, grant agreement #ANR-15-IDEX-02), Noriyuki Isobe (University of Tokyo, Japan) for the chromatography analysis of native amylose, as well as Jacques Pécaut (CEA Grenoble), Karim Mazeau and Henri Chanzy (CERMAV) for stimulating discussions. CERMAV is part of Institut Carnot PolyNat (Investissements d'Avenir, grant agreement #ANR-11-CARN-030-01).

Appendix A. Supplementary data

Supplementary data to this article can be found online at https://doi.org/10.1016/j.polymer.2020.123302.

Abbreviations

BBIOL, butane-1,3-diol; BDIOL, butane-1,4-diol; EDIOL, ethane-1,2-diol; HDIOL, hexane-1,6-diol; MPDIOL, 2-methylpentane-2,4-diol; ED, electron diffraction; TEM, transmission electron microscopy; XRD, X-ray diffraction.

References

[1] J.A. Putseys, L. Lamberts, J.A. Delcour, Amylose-inclusion complexes: Formation, identity and physico-chemical properties, *J. Cereal Sci.* 51 (2010) 238–247, https://doi.org/10.1016/j.jcs.2010.01.011

[2] W.C. Obiro, S.S. Ray, M.N. Emmambux, V-amylose structural characteristics, methods of preparation, significance, and potential applications, *Food Rev. Int.* 28 (2012) 412–438, https://doi.org/10.1080/87559129.2012.660718

[3] D. Lourdin, J.-L. Putaux, G. Potocki-Veronese, C. Chevigny, A. Rolland-Sabaté, A. Buléon, Crystalline structure in starch, in Y. Nakamura (ed.), Starch - Metabolism and Structure, Springer Japan, 2015, pp. 61–90.

[4] B. Conde-Petit, F. Escher, J. Nuessli, Structural features of starch-flavor complexation in food model systems. *Trends Food Sci. Technol.* 17 (2006) 227–235, https://doi.org/10.1016/j.tifs.2005.11.007

[5] F.M. Carbinatto, T.S. Ribeiro, L.A. Colnago, R.C. Evangelista, B.S.F. Cury, Preparation and characterization of amylose inclusion complexes for drug delivery applications. *J. Pharm. Sci.* 105 (2016) 231–241, https://doi.org/10.1002/jps.24702

[6] T.J. Schoch, Fractionation of starch by selective precipitation with butanol. *J. Am. Chem. Soc.* 64 (1942) 2957–2961, https://doi.org/10.1021/ja01264a065

[7] E. Bourne, G. Donnison, N. Haworth, S. Peat, Thymol and cyclohexanol as fractionating agents for starch. *J. Chem. Soc.* (1948) 1687–1693, https://doi.org/10.1039/JR9480001687

[8] T. Kuge, K. Takeo, Complexes of starchy materials with organic compounds: Part II. Complex formation in aqueous solution and fractionation of starch by l-menthone. *Agr. Biol. Chem.* 32 (1968) 1232–1238, https://doi.org/10.1080/00021369.1968.10859210

[9] J. Nuessli, J.-L. Putaux, P. Le Bail, A. Buléon, Crystal structure of amylose complexes with small ligands. Int. *J. Biol. Macromol.* 33 (2003) 227–234, https://doi.org/10.1016/j.ijbiomac.2003.08.009

[10] H. Ades, E. Kesselman, Y. Ungar, E. Shimoni, Complexation with starch for encapsulation and controlled release of menthone and menthol. *LWT Food Sci. Technol.* 45 (2012) 277–288, https://doi.org/10.1016/j.lwt.2011.08.008

[11] J. Singh, N. Singh, S. Saxena, Effect of fatty acids on the rheological properties of corn and potato starch. *J. Food Eng.* 52 (2002) 9–16, https://doi.org/10.1016/S0260-8774(01)00078-4

[12] G.G. Gelders, H. Goesaert, J.A. Delcour, Amylose-lipid complexes as controlled lipid release agents during starch gelatinization and pasting. *J. Agric. Food Chem.* 54 (2006) 1493–1499, https://doi.org/10.1021/jf051743c

[13] A. Marinopoulou, E. Papastergiadis, S.N. Raphaelides, M.G. Kontominas, Morphological characteristics, oxidative stability and enzymic hydrolysis of amylose-fatty acid complexes. *Carbohydr. Polym.* 141 (2016) 106–115, https://doi.org/10.1016/j.carbpol.2015.12.062

[14] T. Oguchi, H. Yamasato, S. Limmatvapirat, E. Yonemochi, K. Yamamoto, Structural change and complexation of strictly linear amylose induced by sealed-heating with salicylic acid. *J. Chem. Soc. Faraday Trans.* 94 (1998) 923–927, https://doi.org/10.1039/A707848J

[15] I. Lalush, H. Bar, I. Zakaria, S. Eichler, E. Shimoni, Utilization of amylose-lipid complexes as molecular nanocapsules for conjugated linoleic acid. *Biomacromolecules* 6 (2005) 121–130, https://doi.org/10.1021/bm049644f

[16] U.V. Lay Ma, J.D. Floros, G.R. Ziegler, Formation of inclusion complexes of starch with fatty acid esters of bioactive compounds. *Carbohydr. Polym.* 83 (2011) 1869–1878, https://doi.org/10.1016/j.carbpol.2010.10.055

[17] L. Zhang, H. Cheng, C. Zheng, F. Dong, S. Man, Y. Dai, P. Yu, Structural and release properties of amylose inclusion complexes with ibuprofen, *J. Drug Delivery Sci. Technol.* 31 (2016) 101–107, https://doi.org/10.1016/j.jddst.2015.12.006

[18] R. St. J. Manley, Chain folding in amylose crystals. *J. Polym. Sci. A* 2 (1964) 4503–4515, https://doi.org/10.1002/pol.1964.100021019

[19] Y. Yamashita, N. Hirai, Single crystals of amylose V complexes. II. Crystals with 7_1 helical configuration. *J. Polym. Sci. A2* 4 (1966) 161–171, https://doi.org/10.1002/pol.1966.160040201

[20] J. Jane, J.F .Robyt, Structure studies of amylose-V complexes and retrograded amylose by action of alpha amylases, and a new method for preparing amylodextrins. *Carbohydr. Res.* 132 (1984) 105–118, https://doi.org/10.1016/0008-6215(84)85068-5

[21] J. Jacob, K. Geßler, D. Hoffmann, H. Sanbe, K. Koizumi, S.M. Smith, T. Takaha, W. Saenger, Band-flip and kink as novel structural motifs in α-(1→4)-D-glucose oligosaccharides. Crystal structures of cyclodeca- and cyclotetradecaamylose. *Carbohydr. Res.* 322 (1999) 228–246, https://doi.org/10.1016/S0008-6215(99)00216-5

[22] J.-L. Putaux, Y. Nishiyama, K. Mazeau, M. Morin, M.B. Cardoso, H. Chanzy, Helical conformation in crystalline inclusion complexes of V-amylose: A historical perspective. *Macromol. Symp.* 303 (2011) 1–9, https://doi.org/10.1002/masy.201150501

[23] J. Brisson, H. Chanzy, W.T. Winter, The crystal and molecular structure of V_H amylose by electron diffraction analysis. *Int. J. Biol. Macromol.* 13 (1991) 31–39, https://doi.org/10.1016/0141-8130(91)90007-H

[24] G. Rappenecker, P. Zugenmaier, Detailed refinement of the crystal structure of Vh-amylose. *Carbohydr. Res.* 89 (1981) 11–19, https://doi.org/10.1016/S0008-6215(00)85225-8

[25] M. Godet, V. Tran, P. Colonna, A. Buléon, M. Pezolet, Inclusion/exclusion of fatty acids in amylose complexes as a function of the fatty acid chain length. *Int. J. Biol. Macromol.* 17 (1995) 405–408, https://doi.org/10.1016/0141-8130(96)81853-8

[26] C.A.K. Le, L. Choisnard, D. Wouessidjewe, J.-L. Putaux, Polymorphism of crystalline complexes of V-amylose with fatty acids. *Int. J. Biol. Macromol.* 119 (2018) 555–564, https://doi.org/10.1016/j.ijbiomac.2018.07.163

[27] W. Helbert, H. Chanzy, Single crystals of V-amylose complexed with n-butanol or n-pentanol: structural features and properties. *Int. J. Biol. Macromol.* 16 (1994) 207–213, https://doi.org/10.1016/0141-8130(94)90052-3

[28] W.-T. Winter, A. Sarko, Crystal and molecular structure of the amylose-DMSO complex. *Biopolymers* 13 (1974) 1461–1482, https://doi.org/10.1002/bip.1974.360130716

[29] T.D. Simpson, X-ray diffraction of ethylenediamine–amylose complex. *Biopolymers* 9 (1970) 1039–1047, https://doi.org/10.1002/bip.1970.360090907

[30] S. Hulleman, W. Helbert, H. Chanzy, Single crystals of V amylose complexed with glycerol. *Int. J. Biol. Macromol.* 18 (1996) 115–122, https://doi.org/10.1016/0141-8130(95)01069-6

[31] B. Biais, P. Le Bail, P. Robert, B. Pontoire, A. Buléon, Structural and stoichiometric studies of complexes between aroma compounds and amylose. Polymorphic transitions and quantification in amorphous and crystalline areas. *Carbohydr. Polym.* 66 (2006) 306–315, https://doi.org/10.1016/j.carbpol.2006.03.019

[32] W. Helbert, Données sur la structure du grain d'amidon et des produits de recristallisation de l'amylose. Doctoral dissertation, 1994, Université Joseph Fourier, Grenoble, France.

[33] Y. Nishiyama, K. Mazeau, M. Morin, M.B. Cardoso, H. Chanzy, J.-L. Putaux, Molecular and crystal structure of 7-fold V-amylose complexed with 2-propanol. *Macromolecules* 43 (2010) 8628–8636, https://doi.org/10.1021/ma101794w

[34] A. Buléon, M.-M. Delage, J. Brisson, H. Chanzy, Single crystals of V amylose complexed with isopropanol and acetone. *Int. J. Biol. Macromol.* 12 (1990) 25–33, https://doi.org/10.1016/0141-8130(90)90078-O

[35] K. Takeo, T. Kuge, Complexes of starchy materials with organic compounds: Part VI. X-ray diffraction of amylose-n-aliphatic ketone complexes. *Agr. Biol. Chem.* 35 (1971) 537–542, https://doi.org/10.1271/bbb1961.35.537
[36] J.-L. Putaux, M.B. Cardoso, D. Dupeyre, M. Morin, A. Nulac, Y. Hu, Single crystals of V-amylose inclusion complexes. *Macromol. Symp.* 273 (2008) 1–8, https://doi.org/10.1002/masy.200851301
[37] C.A.K. Le, J.-L. Putaux, L. Choisnard, D. Wouessidjewe, Single crystals of V-amylose complexed with bicyclic organic compounds. *Macromol. Symp.* 386 (2019) 190007, https://doi.org/10.1021/masy.2019000007
[38] Y. Yamashita, K. Monobe, Single crystals of amylose V complexes. III. Crystals with 8_1 helical configuration. *J. Polym. Sci. A2* 9 (1971) 1471–1481, https://doi.org/10.1002/pol.1971.160090807
[39] M.B. Cardoso, J.-L. Putaux, Y. Nishiyama, W. Helbert, M. Hÿtch, N.P. Silveira, H. Chanzy, Single crystals of V-amylose complexed with α-naphthol. *Biomacromolecules* 8 (2007) 1319–1326, https://doi.org/10.1021/bm0611174
[40] L. Shi, H. Hopfer, G.R. Ziegler, L .Kong, Starch-menthol inclusion complex: Structure and release kinetics. *Food Hydrocoll.* 97 (2019) 105183, https://doi.org/10.1016/j.foodhyd.2019.105183
[41] F. Mikus, R. Hixon, R. Rundle, The complexes of fatty acids with amylose. *J. Am. Chem. Soc.* 68 (1946) 1115–1123, https://doi.org/10.1021/ja01210a062
[42] H.F. Zobel, A.D. French, M.E. Hinkle, X-ray diffraction of oriented amylose fibers. II. Structure of V amyloses. *Biopolymers* 5 (1967) 837–845, https://doi.org/10.1002/bip.1967.360050906
[43] K. Takeo, A. Tokumura, T. Kuge, Complexes of starch and its related materials with organic compounds. Part. X. X-ray diffraction of amylose-fatty acid complexes. *Starch/Stärke* 25 (1973) 357–362, https://doi.org/10.1002/star.19730251102
[44] R.M. Valetta, F.J. Germino, R.E. Lang, R.J. Moshy, Amylose "V" complexes: Low molecular weight primary alcohols. *J. Polym. Sci. A* 2 (1964) 1085–1094, https://doi.org/10.1002/pol.1964.100020306
[45] B. Zaslow, Characterization of a second helical amylose modification. *Biopolymers* 1 (1963) 165–169, https://doi.org/10.1002/bip.360010206
[46] M.A. Rutschmann, J. Solms, Formation of inclusion complexes of starch with different organic compounds. IV, ligand binding and variability in helical conformations of V amylose complexes. *LWT Food Sci. Technol.* 23 (1990) 84–87.
[47] Y.-H. Yamashita, J. Ryugo, K. Monobe, An electron microscopic study on crystals of amylose V complexes. *J. Electron Microsc.* 22 (1973) 19–26, https://doi.org/10.1093/oxfordjournals.jmicro.a049858
[48] F.P. Booy, H. Chanzy, A. Sarko, Electron diffraction study of single crystals of amylose complexed with n-butanol. *Biopolymers* 18 (1979) 2261–2266, https://doi.org/10.1002/bip.1979.360180913
[49] M. Kowblansky, Calorimetric investigation of inclusion complexes of amylose with long-chain aliphatic compounds containing different functional groups. *Macromolecules* 18 (1985) 1776–1779, https://doi.org/10.1021/ma00151a022
[50] MarvinSketch, https://chemaxon.com/products/marvin

[51] J. Laugier, B. Bochu, LMGP-Suite: Suite of programs for the interpretation of X-ray experiments, http://www.ccp14.ac.uk/tutorial/lmgp/
[52] J.D.H. Donnay, Rules for the conventional orientation of crystals. *Am. Mineral.* 28 (1943) 313–328.
[53] K. Takeo, T. Kuge, Complexes of starchy materials with organic compounds: Part III. X-ray studies on amylose and cyclodextrin complexes. *Agr. Biol. Chem.* 33 (1969) 1174–1180, https://doi.org/10.1080/00021369.1969.10859434
[54] J. Bernstein, R.J. Davey, J.-O. Henck, Concomitant polymorphs. *Angew. Chem. Int. Ed.* 38 (1999) 3440–3461.
[55] R.L. Shogren, G.F. Fanta, F.C. Felker, X-ray diffraction study of crystal transformations in spherulitic amylose/lipid complexes from jet-cooked starch. *Carbohydr. Polym.* 64 (2006) 444–451, https://doi.org/10.1016/j.carbpol.2005.12.018
[56] M.E. Hinkle, H.F. Zobel, X-ray diffraction of oriented amylose fibers. III. The structure of amylose-n-butanol complexes. *Biopolymers* 6 (1968) 1119–1128, https://doi.org/10.1002/bip.1968.360060807